Photosensor Device Based on Few-Layered WS_2 Films

*Néstor Perea-López, Ana Laura Elías, Ayse Berkdemir, Andres Castro-Beltran, Humberto R. Gutiérrez, Simin Feng, Ruitao Lv, Takuya Hayashi, Florentino López-Urías, Sujoy Ghosh, Baleeswaraiah Muchharla, Saikat Talapatra, Humberto Terrones, and Mauricio Terrones**

Few-layered films of WS_2, synthesized by chemical vapor deposition on quartz, are successfully used as light sensors. The film samples are structurally characterized by Raman spectroscopy, atomic force microscopy, scanning electron microscopy, and high-resolution transmission electron microscopy. The produced samples consist of few layered sheets possessing up to 10 layers. UV–visible absorbance spectra reveals absorption peaks at energies of 1.95 and 2.33 eV, consistent with the A and B excitons characteristic of WS_2. Current–voltage (*I–V*) and photoresponse measurements carried out at room temperature are performed by connecting the WS_2 layered material with Au/Ti contacts. The photocurrent measurements are carried out using five different laser lines ranging between 457 and 647 nm. The results indicate that the electrical response strongly depends on the photon energy from the excitation lasers. In addition, it is found that the photocurrent varies non-linearly with the incident power, and the generated photocurrent in the WS_2 samples varies as a squared root of the incident power. The excellent response of few-layered WS_2 to detect different photon wavelengths, over a wide range of intensities, makes it a strong candidate for constructing novel optoelectronic devices.

1. Introduction

Layered transition metal dichalcogenides (TMDCs) (e.g., MoS_2 and WS_2) are materials formed by stacked molecular layers interacting via van der Waals forces. Due to the weak van der Waals forces that exist among these layers, it is possible to exfoliate them (chemically or mechanically) in order to obtain single- and few-layers of TMDCs. It has been shown that isolated monolayers of these materials often exhibit physical properties that are very different from their bulk counterpart.[1–5] A good example is MoS_2, which in bulk is an indirect gap semiconductor, however, an isolated monolayer possesses direct band gap, as demonstrated by Mak and co-workers.[1] So far, most of the reports on TMDCs are related to molecular layers obtained by top-down approaches, in which exfoliation from macroscopic crystals is achieved either by mechanical or chemical methods.[6–10] In addition, bottom-up approaches such as the synthesis via chemical vapor deposition (CVD) has been implemented mostly to produce molecular layers of MoS_2.[11–13] Only recently, a CVD method able to obtain triangular islands of monolayered WS_2, exhibiting enhanced photoluminescence from their edges,[14] as well as the controlled growth of large-area films of monolayered WS_2 and MoS_2 and their alloys, have been reported by the Penn State team.[15]

TMDCs are optically active materials due to their semiconducting properties: their band gap matches the visible spectrum. Therefore, these materials have been previously investigated for their use in solar cell applications.[13] Among this family of materials, MoS_2 has been widely used as phototransistor and as an optical detector.[16–19] However, the published literature related to the optical properties and characterization of other TMDC systems such as WS_2, is very scarce. In earlier studies, magnetron sputtering was used to grow WS_2 films.[20,21] These authors reported some of

Dr. N. Perea-López, Dr. A. L. Elías, Dr. A. Berkdemir, A Castro-Beltran, S. Feng, Dr. R. Lv, Dr. F. López-Urías, Prof. H. Terrones, Prof. M. Terrones
Department of Physics and Center for 2-Dimensional and Layered Materials
The Pennsylvania State University
University Park, PA 16802, USA
E-mail: mut11@psu.edu
Dr. H. R. Gutiérrez
Department of Physics & Astronomy
University of Louisville
Louisville, KY 40292, USA

DOI: 10.1002/adfm.201300760

Dr. T. Hayashi, Prof. M. Terrones
Research Center for Exotic Nanocarbons (JST)
Shinshu University
Wakasato 4-17-1, Nagano 380-853, Japan
S. Ghosh, B. Muchharla, Prof. S. Talapatra
Department of Physics
Southern Illinois University Carbondale
IL 62901, USA
Prof. M. Terrones
Department of Chemistry
Department of Materials Science and Engineering and Materials Research Institute
The Pennsylvania State University
University Park, PA 16802, USA

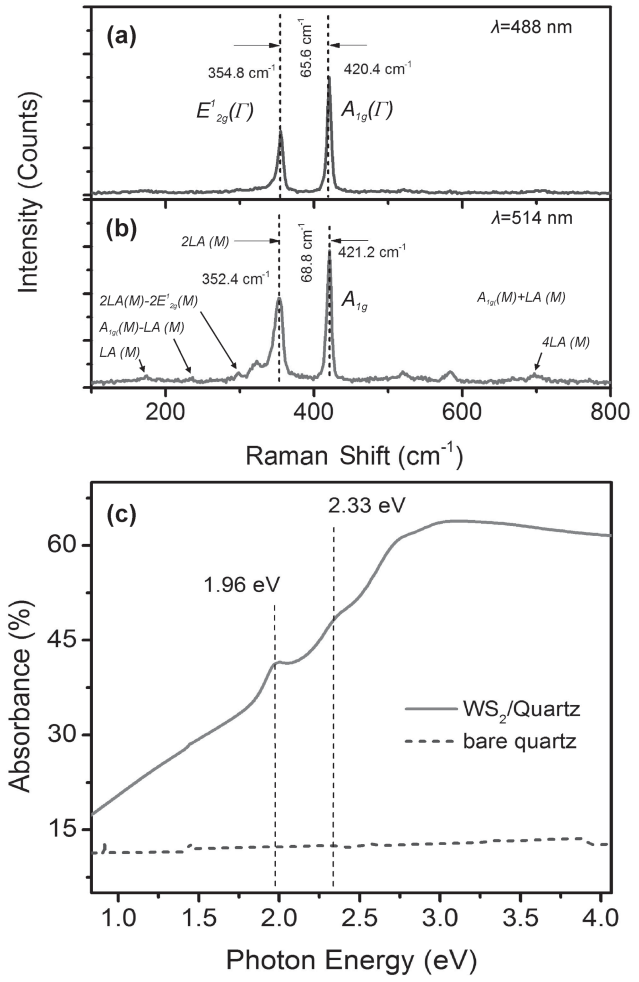

Figure 1. a) Raman spectrum acquired with laser excitation of $\lambda = 488$ nm for the WS_2 film grown on quartz, the Raman shift peaks at 354.8 and 420.4 cm^{-1} are indexed in this spectrum. b) Raman spectrum of the same region as (a) acquired with $\lambda = 514$ nm laser line; notice that additionally to the Raman shift peaks at 352.4 and 421.2 cm^{-1}, there are other Raman peaks. c) Optical absorption spectra obtained from the few layered WS_2 films and from the bare quartz. Two absorption peaks could noticed around 1.96 eV and 2.33 eV; these peaks are associated with the excitonic absorptions A and B of hexagonal WS_2.

the optical, electronic, and semiconducting properties of bulk WS_2. The films they obtained exhibited sizes ranging between 1 and 5 μm and thicknesses from 100 to 200 nm. Magnetron sputtering grown WS_2, revealed p-type behavior with carrier concentration of 10^{23} m^{-3} and very low electron mobility of 1×10^{-3} m^2 V^{-1} s^{-1}. Improved electrical properties were observed for WS_2 nanotubes as reported by Zhang et al.[22] They measured carrier concentration up to 1.6×10^{24} m^{-3} and a vacuum mobility of 7.6×10^{-2} m^2 V^{-1} s^{-1}.[22] More recently, Hwang and collaborators used a chemically synthesized WS_2 flake, around 20 nm thick, to fabricate a Schottky barrier field effect transistor with high on/off current ratio up to 1×10^5.[23]

In this work, we show the behavior of the photocurrent in few-layered WS_2 samples that were grown on quartz by CVD at low pressure. Using this synthesis method, we obtained uniform, continuous, and large area (cm^2) films.[15] The spectral responsivity of few-layered WS_2 films was found to be strongly dependent on the wavelength of the excitation source. For the lower excitation used ($\lambda = 647$ nm; $E = 1.91$ eV) it was found to be 2.0 μA W^{-1}, and for the higher energy used ($\lambda = 568$ nm; $E = 2.71$ eV) it was one order of magnitude higher, 21.2 μA W^{-1}. Regarding the sensitivity, using a wide rang of different excitation intensities, it was found that the photocurrent, $I_P(\Phi)$, was non-linearly related to the power (Φ) of the laser excitation by a function similar to $I_P(\Phi) = b\Phi^{0.5}$, where b is a constant. A photosensitive material with this kind of response has good sensitivity at low intensities and higher sensitivity at intensities orders of magnitude higher, but since the response is saturated, there is no risk of destructive currents, as it usually occurs in inversely polarized diode photodetectors. In order to perform this measurement, the power intensity of the laser line ($\lambda = 514$ nm) was varied from 5×10^{-6} W to 1×10^{-2} W.

2. Results and Discussion

Raman spectroscopy is a very powerful tool to study the structural properties of layered materials and it has had a major role in the rise of graphene.[24] In particular, Raman spectra of the produced few-layered WS_2 films, for two different laser excitations, are depicted in **Figure 1**. For MoS_2, it has been recently found that the frequency difference between the Raman peaks could be accurately related to the number of layers when 488 nm excitation laser was used.[25] Although WS_2 exhibits a rather similar crystal structure when compared to MoS_2, recent Raman spectroscopy measurements indicate that the 514 nm laser line results in the lattice resonance of WS_2 monolayers, thus rendering a strong resonant peak 2LA(M) located very close to the E^1_{2g}. From these findings, it was concluded that the intensity ratio between the A_{1g} and the 2LA(M) Raman peaks for WS_2 could be linked to the number of layers within the synthesized film, using the laser excitation of 514 nm.[26] However, in order to discriminate few layered samples from the bulk (infinite layers), it is necessary to record the background signal of the silicon substrate; the ratio between the E^1_{2g} peak of the TMDC and the Si peak (≈520 cm^{-1}) can be used to estimate the thickness of few-layered ($N > 3$) TMDCs samples.[11,26] In the case of these few-layered WS_2 films grown on quartz, there was no background silicon peak in the Raman spectrum to estimate the number of atomic layers, because of this situation atomic force microscopy (AFM) was used to obtain the sample thickness (see below). Figure 1a depicts the Raman data for the 488 nm laser excitation; the peak position difference between E^1_{2g} and A_{1g} modes indicates that the sample consists of multiple layers. The observed Raman peaks are located at 354.8 and 420.4 cm^{-1}. For the 514 nm laser excitation, the E^1_{2g} and the A_{1g} Raman peaks occurred at 352.4 and 421.2 cm^{-1}, respectively, and additional peaks in the Raman spectrum were also noticeable and were assigned in the spectrum (see Figure 1a).[27] The Raman spectra in Figure 1 were acquired in the active channel region of one of the WS_2 fabricated devices, exactly between the Au/Ti electrodes described in the device fabrication experimental section. In Figure 1c, the optical absorption spectra of the few-layered WS_2 film and the bare quartz are presented; the quartz substrate displays very small absorption

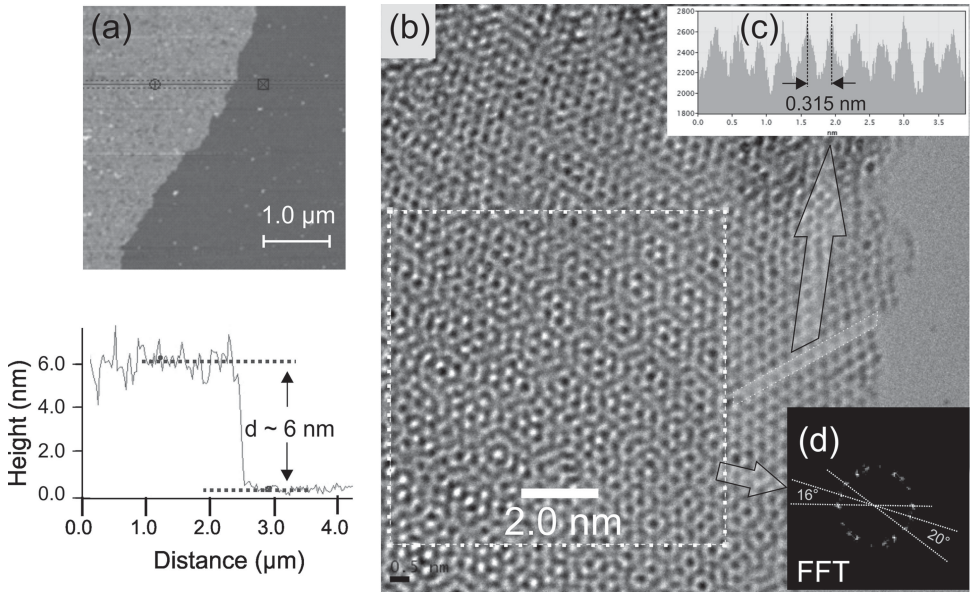

Figure 2. a) Atomic force microscopy image of few layered WS_2 film edges transferred to SiO_2/Si. From the topography profile (see the height vs. distance plot along the red line), a thickness around 6 nm could be determined, indicating a thickness of 10 layers approximately. b) HRTEM image showing a well formed hexagonal structure. c) Line scan profile in which the lattice parameter $b \approx 0.315$ nm was measured. d) Fast Fourier transformation (FFT) from the region indicated by the arrow in which at least 3 layers of WS_2 are stacked in different orientation angles.

and the spectrum is almost flat along the near UV and visible range between 200 and 900 nm (4.0 eV to 1.2 eV). For the same spectral range, the few-layered WS_2 sheet exhibits high absorption in the near UV region (E > 3 eV) and, in the visible region (1.3 eV < E < 3.0 eV), the absorbance decreases as the photon energy becomes smaller. In addition, in the visible region, the absorbance curve has two notable features (shoulders) located at 2.33 and 1.96 eV, that are related to the direct band transitions of WS_2 and matched the characteristic excitons A and B.[21,28]

In order to estimate the in plane continuity, as well as number of layers of the grown WS_2 samples, we have performed atomic force microscopy (AFM) measurements (see **Figure 2**a). AFM height profiles were carried out on the WS_2 films. From these results, it was clearly noticed that the films were continuous exhibiting thicknesses around 6 nm (≈10 layers). In order to perform the high resolution transmission electron microscopy (HRTEM) characterization the synthesized $WS_2/SiO_2/Si$ films were transferred to a Quantifoil grid. For the lift off process, the SiO_2 was dissolved using concentrated hydrofluoric acid (ACS, 48–51%, Alfa Aesar, CAS 7664-39-3), and the WS_2 films were lifted with standard polymethyl methacrylate (PMMA) coating, used for graphene samples.[29] Figure 2b shows the HRTEM images of the few-layered WS_2, in which the contrast allows the determination of the unit cell dimensions. Figure 2c depicts the contrast profile recorded along the blue line (see the arrow in Figure 2b). The fast Fourier transform (FFT) is also shown in Figure 2d, indicating that the multiple layers are rotated with respect to each other, by 16 and 20 degrees. At this stage, it is not clear how this rotation occurred and it might possible that such rotations are inherent to the growth process; alternatively, they could be caused after the film transfer process.

Figures 3a depicts a schematic representation of the device components; it shows the WS_2 film, Au/Ti contacts, quartz substrate and the laser beam interacting with the layered material. The electrical contacts made of Au/Ti films were deposited by an e-beam evaporator. A stainless steel shadow mask was used to pattern electrode pads 0.5 mm × 1 mm spaced 50 micrometers apart; those electrical contacts were connected to macroscopic electrodes using indium and gold wire as can be appreciated in the false color scanning electron microscopy (SEM) image in Figure 3b; the substrates containing the WS_2 film and electrodes were attached to chip carrier fixtures for electrical testing. The current–voltage plot in absence of laser beam is shown in Figure 3c. A basic resistance versus temperature characterization was obtained on the measured samples. In general, these devices presented resistances in the order of few mega Ohms at room temperature; one of the samples, which exhibited a resistance of ≈3 MΩ, was used to measure the behavior of the devices at low temperatures. The variation of resistance with temperature in the range 120 K < T < 320 K was recorded for a few-layered WS_2 film with top contacted Ti/Au on quartz as those used for the photocurrent measurements. The data indicate a non-linear increase of the resistance with decreasing temperature, also known as negative temperature coefficient of resistivity (TCR). Overall, the variation of the resistance for the WS_2 layers could be broken down into two distinct temperature regimes. At higher temperatures (from 320 K to $T \approx 200$ K), the resistance of the few-layered WS_2 increased slowly with decreasing temperature but, below 200 K, the resistance sharply increased (see Figure 3d). Such nonlinear temperature-dependence of the resistivity, with negative TCR, has been observed for other 2D electronic systems, and it is consistent with the semiconducting nature of this dichalcogenide material (WS_2).

The optical excitation was then supplied using the 50× objective of the optical microscope installed in the via Renishaw Raman spectrometer. The variation of the current flowing

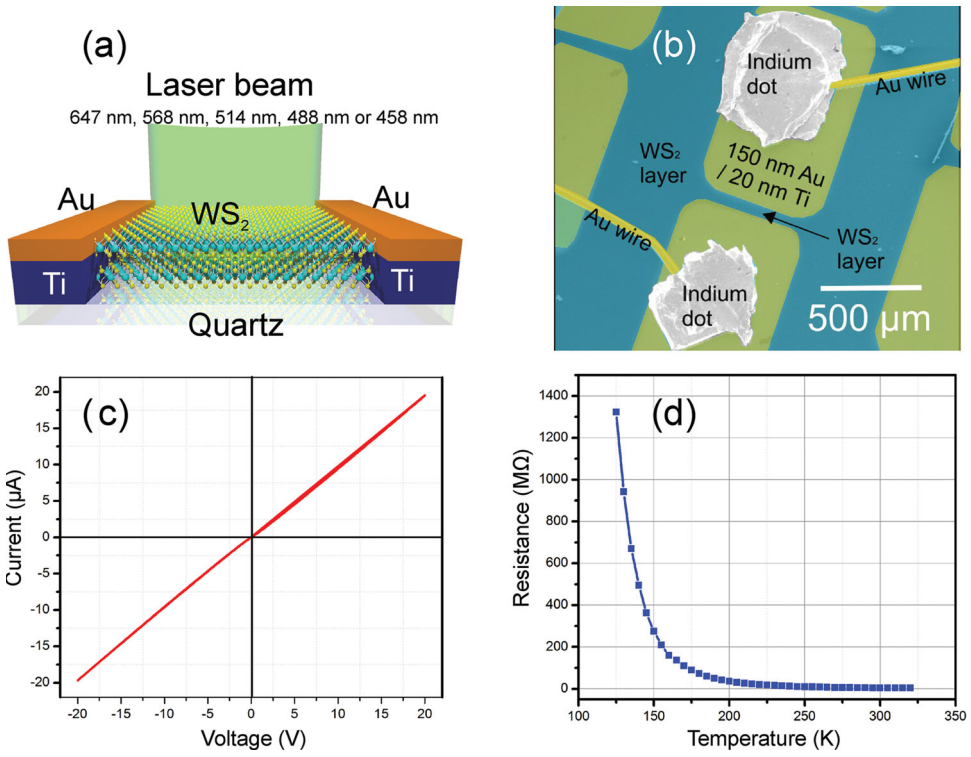

Figure 3. a) Schematic representation of the photo detector device consisting of a few-layered WS_2 film on quartz, the Au/Ti contacts and the different laser wavelengths were applied perpendicularly to the film. b) Colored SEM image showing the device electrical connections made with Au micro wire glued with metallic Indium dots. c) Current–voltage plot obtained in absence of laser beam (darkness condition). d) The variation of resistance with temperature (120 K < T < 320 K) for a WS_2 sample with top contacted Ti/Au on quartz substrate, similar to a device shown in (b).

through the film was monitored with the power source-meter. In all the photocurrent measurements the photocurrent was the time varying component on top of from a direct current (DC) level; the photocurrent was produced by switching the laser beam on and off for arbitrary time intervals. **Figure 4**a shows photocurrent versus applied voltage plots; the measurements were carried by sweeping the applied voltage from 1 V to 30 V. In addition, three different illumination intensities were applied to the WS_2 device at powers of 0.65 mW, 3.25 mW, and 6.25 mW. Such power values were confirmed with a hand held continuous wave (CW) laser power meter (Edmund Optics ± 5% accuracy). These I–V plots show linear increase of the photocurrent with the applied voltage. In Figure 4b, the dependence of the photocurrent (in μA) to the laser power irradiation (Φ in W), was plotted in a log–log scale. By extracting the slope of this plot, a nonlinear dependence of the photocurrent was found. The dependence was close to $b\Phi^{0.5}$, in which b is a constant and Φ is the laser power; a remarkable feature observed in this plot was the wide range of detection at illumination powers ranging from 5×10^{-6} W to 1×10^{-2} W. Figure 4c depicts the spectral responsivity of the WS_2 device as a function of the wavelength of the laser excitation. A clear trend could be noted since higher energy lasers induce large photocurrents. The smallest spectral photoresponse corresponded to 2.0 μA W^{-1}, a value measured for the red laser with a wavelength of 647 nm (1.92 eV), and the highest recorded photoresponse corresponded to 21.2 μA W^{-1}, measured with the blue laser (λ = 458 nm; E = 2.71 eV). The output power of all the used laser lines was fixed to 2.0 mW prior to the photocurrent measurements.

Regarding the stability of the photocurrent response, an extended duration photocurrent measurement was performed by switching the laser on and off; the duration at the on state was sustained during 40 seconds, **Figure 5**d shows the photocurrent stability over almost one hour of continuous operation; there were oscillations in the direct current (DC) level and those oscillations were suppressed in the data of Figure 4b. However, it is still possible to notice that the photocurrent response is very stable since there is no significant variation on the signal amplitude. The slow variations of the DC level can be produced by thermal drift produced by the heat accumulation on the device, since it is assembled on a thermally insulating substrate. Furthermore, in order to investigate the fast response of the photocurrent, an optical chopper was introduced on the laser path to produce laser pulses with duration of 20×10^{-3} s. The electrical response of the WS_2 device is shown in Figure 5; the waveform was acquired with an oscilloscope capable to acquire signals up to 100 MHz. The photocurrent signal revealed symmetric rise and fall times with value close to 5.3×10^{-3} s. This value is, to the best of our knowledge, the fastest observed in layered materials photodetectors (e.g., MoS_2,WS_2, GaSe).

Table 1 includes the comparison of important device parameters as photocurrent amplitude, the responsivity, and the response time, including the results here obtained and homologous MoS_2 few- and monolayer devices. A comparison to ZnO nanoneedles is also made. Comparing the responsivity

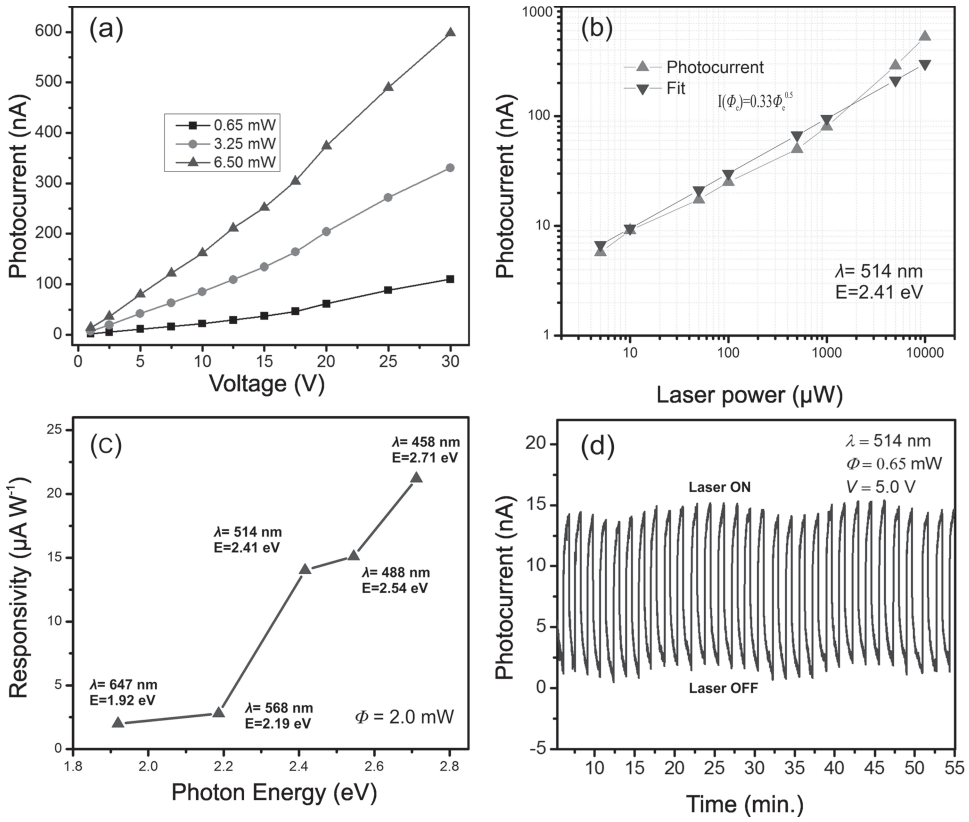

Figure 4. Photosensor device characterization. a) Photocurrent vs. voltage plots acquired with different laser power irradiation of 0.65, 3.25, and 6.5 mW; in this power and voltage range, the current was found to depend linearly on the applied voltage. b) Photocurrent vs. laser power plot in which the current was found to depend non-linearly on the radiant power as $\Phi^{0.5}$. c) Responsivity plot for different laser wavelengths. It can be clearly noticed that the shorter wavelengths (higher energies) result in larger photocurrents (≈22 μA W^{-1} for the 458 nm laser line). d) Device current vs. time with alternated turn-on and turn-off laser beam pulse; good stability of the photocurrent response after almost 1 hour of operation with 40 s duty cycles. The laser beam wavelength corresponded to 514 nm at 0.65 mW and the device was polarized with 5.0 V. Notice that the time periods when the laser status was ON, the current increases sharply.

(R) of the different devices reported in literature is complicated if we consider that R is a function of the irradiation intensity (Φ) as $R = I_P/\Phi$, but the photocurrent (I_P) is itself a function of the irradiation intensity as $I_P = b\Phi^{0.5}$; then, R can be calculated as a function the irradiation intensity, as $R = b\Phi^{-0.5}$. According to this function, small values of irradiation will yield very high responsivities. Meanwhile, high illumination intensities will show smaller values. This makes the comparison between reported devices complicated since the device dimensions vary from a report to the next and the illumination sources used can vary greatly as well. An important parameter that can define the quality of the photosensor is the response time; in this matter, the results obtained here are the best, one order of magnitude faster than the previous reports. In general, the characterization of the response time of the devices presented in literature is obtained from very slow on and off illumination intervals, in the order of seconds and up to tens of seconds, hence limiting the extraction of the fast response from that data. In this report, we used 20×10^{-3} s train pulses generated with an optical chopper to study the fast response of the device. It was found that the rise and fall times are equal and close to 5.3×10^{-3} s (see Figure 5).

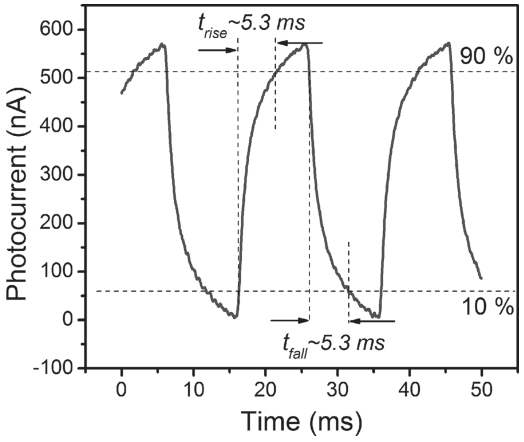

Figure 5. Time response of the WS_2 photosensor device obtained using an optical chopper tuned at 50 Hz to produce laser beam pulses with 20 ms duration. By reading the waveform in an oscilloscope, the rise and fall times were measured to be close to 5.3 ms.

The use of monolayers of WS_2 (CVD-grown)[14] neither showed good transport measurement results nor photodetection. The single layer devices constructed appeared to be very resistive (GΩ range), possibly due to Shottky barrier effects

Table 1. Comparison of important device characteristics of this work and photodetectors based on other layered materials and ZnO nano needles.

Material	Device architecture	Photocurrent[a] I_{Pmax}	Responsivity	Spectral range	Response time	Ref.
Multilayer WS_2	2 terminal	≈600 nA	≈92 μA W^{-1}	Visible	5.3×10^{-3} s	This work
Multilayer WS_2	3 terminal FET	≈90 nA	ND	Visible	ND, few seconds	[23]
Multilayer MoS_2	3 terminal FET	≈30 nA	≈150 mA W^{-1}	Visible	ND	[28]
Monolayer and Multilayer MoS_2	3 terminal FET top gated	≈3 nA	ND	UV-Visible	1L 1.5 s 2L 1.0 s 3L 0.3 s	[17]
Multilayer MoS_2	3 terminal FET bottom gated	≈180 nA	7.5 mA W^{-1}	UV-Vis	50×10^{-3} s	[16]
Multilayer GeSe	3 terminal FET bottom gated	≈0.8 nA	ND	Visible	few seconds	[10]
Single needle ZnO	2 terminal	≈100 000 nA	ND	UV	≈1 s	[30]
Single needle ZnO	3 terminal FET	≈10 nA	4700 A W^{-1}	UV	ND	[31]
Single needle ZnO	3 terminal FET	≈120 nA	ND	Visible	Few seconds	[32]
Multiple ZnO needles	2 terminal	≈1.5 mA@UV ≈10 nA@blue	ND	325 nm and 458 nm	≈0.3 s	[33]

[a]Maximum value reported on the experimental data.

established between the electrodes and the WS_2 monolayer. Various attempts to deposit contacts on monolayers were unsuccessful, including Pt, Au/Cr, Au/Ti, W, and Ni, and these devices revealed very high resistances in the range between 10×10^8 and 1×10^{12} Ω. *I–V* plots and images of these devices are presented in Figure S1, Supporting Information. Recently, Choi and co-workers reported that a similar situation occurs with MoS_2, demonstrating that a photodetector using multilayer MoS_2 exfoliated from bulk crystals could exhibit superior performance when compared to single-layer crystal flakes.[28]

3. Conclusions

We have demonstrated that few-layered WS_2 films could be used as a wavelength sensitive photo detector at room temperature. The WS_2 films were synthesized by CVD and characterized by Raman spectroscopy, AFM, SEM, and HRTEM. We demonstrated by AFM that the synthesized films were continuous and consisted of few-layers exhibiting thicknesses of approximately 6 nm (10 layers approximately). The peak position and intensity ratio between the E^1_{2g} and A_{1g} modes observed in the Raman spectrum confirms the thickness measured by AFM. The optical absorbance results demonstrated the presence of A and B excitons characteristic of WS_2. The fabricated sensor device was tested for different photon energy excitations. The photocurrent was monitored as a function of time with an alternating ON and OFF laser beam illumination. It was noted that the photocurrent appeared when the laser beam was allowed to illuminate the device and it revealed strong dependence on the wavelength and on the illumination power. The fast response of the device was also measured and resulted in 5.3 ms for rise and fall times, the fastest response reported so far for transition few layered metal dichalcogenide devices. Because of its fast response, good responsivity, and stability, it is envisaged that few-layered WS_2 films could be important components of future optoelectronic devices.

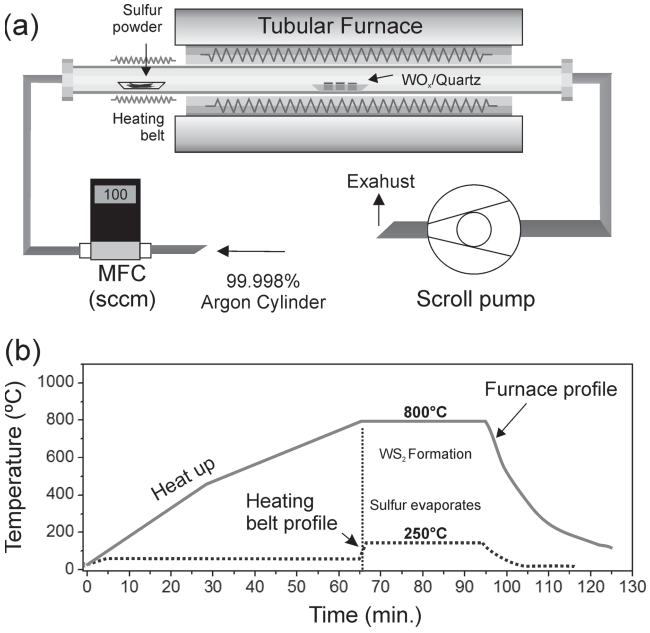

Figure 6. Chemical vapor deposition (CVD) method set up used for the synthesis of continuous few-layered WS_2 films. a) A quartz tube used to host the sulfur powder and the substrates with an ultra-thin WO_x layer. A heating belt was used to evaporate the sulfur powder and the high temperature furnace kept the WO_x substrate at 800 °C. The sulfur vapor is dragged by an Argon flow controlled by a mass-flow controller (MFC) at 100 sccm. b) Temperature profiles for the heating belt and the furnace during the synthesis of few layered WS_2.

4. Experimental Section

WS_2 continuous films were fabricated by CVD involving the sulfurization of ultra-thin tungsten oxide films. Briefly, the oxidized films are deposited on quartz and SiO_2/Si substrates (Ted Pella Inc. and Nova electronics Inc.) by thermal evaporation from the oxide powders (WO_3, alfa aesar 99.99%), using a high vacuum evaporator (KJ Lesker PVD-75). After the oxide deposition, the substrates were loaded in a tubular reactor for a subsequent sulfurization at 800 °C for 30 min; see **Figure 6**a and the

temperature profile shown in Figure 6b. After the CVD process, the films grown on quartz were characterized by Raman spectroscopy, UV-visible spectroscopy, atomic force microscopy (AFM), and scanning electron microscopy (SEM). Additionally, some WS_2 samples were grown on 285 nm SiO_2/Si and used for transfers in order to perform HRTEM. The photocurrent measurements were carried out at room temperature using a vacuum chamber at pressures of 1×10^{-6} Torr, and were coupled to a micro Raman spectrometer (Renishaw). The different laser excitation lines were selected from an Argon ion laser (Innova 70C Spectrum). The electrical conduction data was collected with a power source and a meter (Keithley 2400). The resistance versus temperature was plotted using VersaLab instrument manufactured by quantum design.

Supporting Information

Supporting Information is available from the Wiley Online Library or from the author.

Acknowledgements

This work is supported by the U.S. Army Research Office MURI grant W911NF-11-1-0362, by the Materials Simulation Center of the Materials Research Institute, the Research Computing and Cyberinfrastructure unit of Information Technology Services and Penn-State Center for Nanoscale Science. M.T. thanks JST-Japan for funding the Research Center for Exotic NanoCarbons, under the Japanese regional Innovation Strategy Program by the Excellence. M.T. also acknowledges support from the Penn State Center for Nanoscale Science for seed grant on 2-D Layered Materials (DMR-0820404). Research was carried out in part at CFN, Brookhaven National Laboratory, which is supported by the US Department of Energy, Office of Basic Energy Sciences, under contract No. DE-AC02-98CH10886. The authors also acknowledge the Center for 2D Materials at PSU.

Received: February 28, 2013
Revised: April 1, 2013
Published online: June 12, 2013

[1] K. F. Mak, C. Lee, J. Hone, J. Shan, T. F. Heinz, *Phys. Rev. Lett.* **2010**, *105*, 136805.
[2] Q. H. Wang, K. Kalantar-Zadeh, A. Kis, J. N. Coleman, M. S. Strano, *Nat. Nanotechnol.* **2012**, *7*, 699.
[3] H. S. S. R. Matte, A. Gomathi, A. K. Manna, D. J. Late, R. Datta, S. K. Pati, C. N. R. Rao, *Angew. Chem. Int. Ed.* **2010**, *49*, 4059.
[4] G. Eda, T. Fujita, H. Yamaguchi, D. Voiry, M. W. Chen, M. Chhowalla, *ACS Nano* **2012**, *6*, 7311.
[5] T. Korn, G. Plechinger, S. Heydrich, M. Hirmer, F. X. Schrettenbrunner, D. Weiss, J. Eroms, C. Schuller, *Proc. SPIE* **2012**, *8456*, 84560H-1.
[6] R. J. Smith, P. J. King, M. Lotya, C. Wirtz, U. Khan, S. De, A. O'Neill, G. S. Duesberg, J. C. Grunlan, G. Moriarty, J. Chen, J. Z. Wang, A. I. Minett, V. Nicolosi, J. N. Coleman, *Adv. Mater.* **2011**, *23*, 3944.
[7] Z. Y. Zeng, Z. Y. Yin, X. Huang, H. Li, Q. Y. He, G. Lu, F. Boey, H. Zhang, *Angew. Chem. Int. Ed.* **2011**, *50*, 11093.
[8] W. Zhao, Z. Ghorannevis, L. Chu, M. Toh, C. Kloc, P.-H. Tan, G. Eda, *ACS Nano* **2012**, *7*, 791.
[9] S. X. Wu, Z. Y. Zeng, Q. Y. He, Z. J. Wang, S. J. Wang, Y. P. Du, Z. Y. Yin, X. P. Sun, W. Chen, H. Zhang, *Small* **2012**, *8*, 2264.
[10] D. J. Xue, J. H. Tan, J. S. Hu, W. P. Hu, Y. G. Guo, L. J. Wan, *Adv. Mater.* **2012**, *24*, 4528.
[11] Y. J. Zhan, Z. Liu, S. Najmaei, P. M. Ajayan, J. Lou, *Small* **2012**, *8*, 966.
[12] Y.-H. Lee, X.-Q. Zhang, W. Zhang, M.-T. Chang, C.-T. Lin, K.-D. Chang, Y.-C. Yu, J. T.-W. Wang, C.-S. Chang, L.-J. Li, T.-W. Lin, *Adv. Mater.* **2012**, *24*, 2320.
[13] M. Shanmugam, C. A. Durcan, B. Yu, *Nanoscale* **2012**, *4*, 7399.
[14] H. R. Gutiérrez, N. Perea-López, A. L. Elías, A. Berkdemir, B. Wang, R. Lv, F. López-Urías, V. H. Crespi, H. Terrones, M. Terrones, *Nano Lett.* **2012**, DOI: 10.1021/nl3026357.
[15] A. L. Elias, N. Perea-Lopez, A. Castro-Beltran, A. Berkdemir, R. Lv, S. Feng, L. A. T. Hayashi, Y. A. Kim, M. Endo, N. Pradhan, L. Balicas, T. E. Mallouk, F. Lopez-Urias, H. Terrones, M. Terrones, *ACS Nano* **2013**, DOI: 10.1021/nn400971k.
[16] Z. Y. Yin, H. Li, H. Li, L. Jiang, Y. M. Shi, Y. H. Sun, G. Lu, Q. Zhang, X. D. Chen, H. Zhang, *ACS Nano* **2012**, *6*, 74.
[17] H. S. Lee, S. W. Min, Y. G. Chang, M. K. Park, T. Nam, H. Kim, J. H. Kim, S. Ryu, S. Im, *Nano Lett.* **2012**, *12*, 3695.
[18] H. S. Lee, S. W. Min, M. K. Park, Y. T. Lee, P. J. Jeon, J. H. Kim, S. Ryu, S. Im, *Small* **2012**, *8*, 3111.
[19] B. Radisavljevic, A. Radenovic, J. Brivio, V. Giacometti, A. Kis, *Nat. Nanotechnol.* **2011**, *6*, 147.
[20] C. Ballif, M. Regula, P. E. Schmid, M. Remskar, R. Sanjines, F. Levy, *Appl. Phys. A: Mater. Sci. Process.* **1996**, *62*, 543.
[21] C. Ballif, M. Regula, F. Levy, *Sol. Energy Mater. Sol. Cells* **1999**, *57*, 189.
[22] C. Y. Zhang, S. Wang, L. J. Yang, Y. Liu, T. T. Xu, Z. Y. Ning, A. Zak, Z. Y. Zhang, R. Tenne, Q. Chen, *Appl. Phys. Lett.* **2012**, *100*, 243101.
[23] W. S. Hwang, M. Remskar, R. S. Yan, V. Protasenko, K. Tahy, S. D. Chae, P. Zhao, A. Konar, H. L. Xing, A. Seabaugh, D. Jena, *Appl. Phys. Lett.* **2012**, *101*, 013107.
[24] A. C. Ferrari, J. C. Meyer, V. Scardaci, C. Casiraghi, M. Lazzeri, F. Mauri, S. Piscanec, D. Jiang, K. S. Novoselov, S. Roth, A. K. Geim, *Phys. Rev. Lett.* **2006**, *97*, 187401.
[25] S. Najmaei, Z. Liu, P. M. Ajayan, J. Lou, *Appl. Phys. Lett.* **2012**, *100*, 013106.
[26] A. Berkdemir, H. R. Gutierrez, A. R. Botello-Mendez, N. Perea-Lopez, A. L. Elias, C.-I. Chia, B. Wang, V. H. Crespi, F. Lopez-Urias, J. C. Charlier, H. Terrones, M. Terrones, *Sci. Rep.* **2013**, *4*, 1755.
[27] G. L. Frey, R. Tenne, M. J. Matthews, M. S. Dresselhaus, G. Dresselhaus, *J. Mater. Res.* **1998**, *13*, 2412.
[28] W. Choi, M. Y. Cho, A. Konar, J. H. Lee, G. B. Cha, S. C. Hong, S. Kim, J. Kim, D. Jena, J. Joo, S. Kim, *Adv. Mater.* **2012**, *24*, 5832.
[29] R. Lv, Q. Li, A. R. Botello-Méndez, T. Hayashi, B. Wang, A. Berkdemir, Q. Hao, A. L. Elías, R. Cruz-Silva, H. R. Gutiérrez, Y. A. Kim, H. Muramatsu, J. Zhu, M. Endo, H. Terrones, J.-C. Charlier, M. Pan, M. Terrones, *Sci. Rep.* **2012**, *2*.
[30] D. Park, K. Yong, *J. Vac. Sci. Technol. B* **2008**, *26*, 1933.
[31] W. Y. Weng, S. J. Chang, C. L. Hsu, T. J. Hsueh, *ACS Appl. Mater. Inter.* **2011**, *3*, 162.
[32] Z. Y. Fan, P. C. Chang, J. G. Lu, E. C. Walter, R. M. Penner, C. H. Lin, H. P. Lee, *Appl. Phys. Lett.* **2004**, *85*, 6128.
[33] K. Keem, H. Kim, G. T. Kim, J. S. Lee, B. Min, K. Cho, M. Y. Sung, S. Kim, *Appl. Phys. Lett.* **2004**, *84*, 4376.